Image recovery via geometrically structured approximation

Hui Ji[a,*], Yu Luo[b,a], Zuowei Shen[a]

[a]*Department of Mathematics, National University of Singapore, Singapore 117543*
[b]*School of Computer and Engineering, South China University of Technology, Guangzhou, China*

Abstract

In recent years, the ℓ_1 norm based regularization has been one promising technique for solving many ill-posed inverse problems in image recovery. As the performance gain of these methods over linear methods comes from the separate process for smooth image regions and image discontinuities, their performance largely depends on how accurate such separation is. However, there is a lot of ambiguities between smooth image regions and image discontinuities when only degraded images are available. This paper aims at developing new wavelet frame based image regularization to resolve such ambiguities by exploiting geometrical regularities of image discontinuities. Based on the geometrical connectivity constraint on image discontinuities, an alternating iteration scheme is proposed which is simple in implementation and efficient in computation. The experiments show that the results from the proposed regularization method are compared favorably against that from several existing ℓ_1 norm or ℓ_0 norm based image regularizations.

Keywords: wavelet tight frame, sparse approximation, image recovery

1. Introduction

Image recovery is one fundamental process with a wide range of applications. Image recovery aims at recovering an image of high-quality from its degraded measurement with noise. The degraded measurement $\mathbf{g}$ is often modeled by applying a linear operator $\mathbf{A}$ to the original signal $\mathbf{f}$:

$$\mathbf{g} = \mathbf{A}\mathbf{f} + \boldsymbol{\epsilon}, \tag{1}$$

where $\boldsymbol{\epsilon}$ denotes the measurement noise which is typically assumed to be white Gaussian noise. In most image restoration tasks, the linear operator $\mathbf{A}$ is either ill-posed or non-invertible thus a straightforward inversing process will either significantly amplify the noise or generating artifacts in the solution. For example, for image deblurring, $\mathbf{A}$ is a convolution operator by a low-pass filter that will significantly attenuate/erase

*Corresponding author
Email addresses: matjh@nus.edu.sg (Hui Ji), matluoy@nus.edu.sg (Yu Luo), matzuows@nus.edu.sg (Zuowei Shen)

high-frequency components of an image. For image inpainting, $\mathbf{A}$ is a projection operator that maps the full set of image pixels to its subset. To solve these ill-posed image restoration problems, certain prior information of the image for recovery is needed to regularize the recovery process.

By assuming that images can be well approximated by smooth functions, traditional linear methods, e.g. Tikhonov regularizations, find the solution of (1) via solving a squared ℓ_2 norm based minimization:

$$\min_{\mathbf{f}} \|\mathbf{A}\mathbf{f} - \mathbf{g}\|_2^2 + \lambda\|\mathbf{\Gamma}\mathbf{f}\|_2^2, \tag{2}$$

where $\mathbf{\Gamma}$ is an operator such that the coefficients $\mathbf{\Gamma}\mathbf{f}$ are close to zero. One often used operator is the difference operator. However, most images of interest cannot be well approximated by smooth functions, as the content of an image is actually dominated by image edges which show rapid intensity changes in its neighborhood. Due to omitting image discontinuities, image edges in the solution obtained from (2) are usually smoothed out.

Suppose the locations of image discontinuities are known with oracles, then the image $\mathbf{f}$ can be recovered with sharp image edges by solving the following optimization problem:

$$\min_{\mathbf{f}} \|\mathbf{A}\mathbf{f} - \mathbf{g}\|_2^2 + \lambda\|(\mathbf{\Gamma}\mathbf{f})_{\Omega^c}\|_2^2. \tag{3}$$

where Ω is th1e index set of image pixels on image discontinuities, and Ω^c denotes its complement. Thus, as long as there are sufficient entries in Ω^c, the solution from (3) is a well-posed one, and image discontinuities are well kept in the solution. Clearly, the critical part in (3) is then how to accurately estimate the index set Ω, or equivalently, how to accurately detect the locations of image discontinuities. For image recovery, such a task is a difficult one as only degraded images are available.

1.1. Treatment of image discontinuities in existing methods

The concept of (3) is indeed implicitly utilized in the ℓ_1 norm based regularizations, which generally yield better results than the Tikhonov regularization (2). The most often used ℓ_1 norm based regularization to find the solution of (1) is by solving the following optimization problem:

$$\frac{1}{2}\|\mathbf{A}\mathbf{f} - \mathbf{g}\|_2^2 + \lambda\|\mathbf{\Gamma}\mathbf{f}\|_1, \tag{4}$$

where $\mathbf{\Gamma}$ is some operator such that most entries of $\mathbf{\Gamma}\mathbf{f}$ are zeros or close to zero. The most often seen operators include difference operators with different orders and the analysis operators of wavelet frames. It can be seen that when images are well approximated by piece-wise smooth functions, the values of $\mathbf{\Gamma}\mathbf{f}$ on smooth image regions will be zero or close to zero and the values of $\mathbf{\Gamma}\mathbf{f}$ on image discontinuities will have large magnitude. As ℓ_1 norm can be used as a sparsity-prompting function [9, 21], the model (4) seeks a solution that have a small percentage of entries with large magnitude and expects the pixels corresponding to these entries are exactly on image discontinuities. However, for smooth image regions, the penalty of ℓ_1 norm is often not large enough to avoid those estimations with some artificial discontinuities. As a result, the model (4)

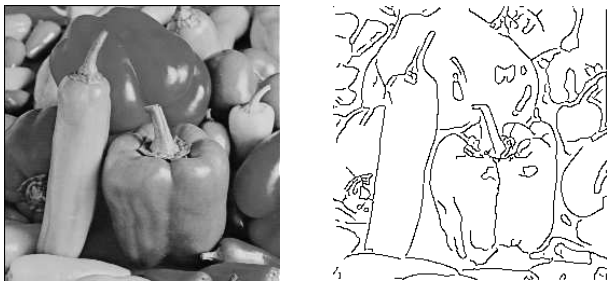

(a) original image $\mathbf{f}$ (b) binary image of $\mathbf{\Gamma f}$

Figure 1: The illustration of the support of image discontinuities.

sometimes introduces un-wanted artifacts, e.g. artificial image edges in smooth image regions.

The concept of (3) is explicitly exploited in the optimization model proposed in [2] for recovering images with piece-wise smoothness:

$$\min_{\Omega,\mathbf{f}} \frac{1}{2}\|\mathbf{Af}-\mathbf{g}\|_2^2 + \lambda\|(\mathbf{Wf})_{\Omega^c}\|_2^2 + \mu\|(\mathbf{Wf})_{\Omega}\|_1, \tag{5}$$

where $\mathbf{W}$ denotes the analysis operator of a wavelet tight frame in high-pass channels, and Ω denotes the index set of the entries of $\mathbf{Wf}$ with significant magnitude. As image discontinuities can be well modeled by wavelet frame coefficients with large magnitude, the model (5) uses the square of ℓ_2 norm to regularize the recovery of smooth image regions and uses ℓ_1 norm to regularize the recovery of image edges. Another one that exploits the similar idea is the so-called *co-sparsity* model introduced in [32], which also solves the ill-posed linear system (1) by (3). As the model (3) requires the knowledge of the support of $\mathbf{\Gamma f}$, the following ℓ_0 norm based model is proposed in [32] for the noise-free case:

$$\min \|\mathbf{\Gamma f}\|_0, \quad \text{subject to} \quad \mathbf{Af} = \mathbf{g}. \tag{6}$$

Although both model (5) and (6) showed some improvement over the classic model (4) when processing images of relatively simple structures. The performance gain on images of complex structures is relatively minor and the performance bottleneck lies in the accurate detection of image discontinuities when only degraded images are available. Taking blurred image for example, many image discontinuities are smoothed out in the input blurry images. If using some not-so-great de-blurred results for estimation, the artificial image discontinuities in these results will lead to wrongly identified image discontinuities. In other words, there exists a lot of ambiguities on the locations of image discontinuities. In order to have more powerful regularization methods for image recovery, there is a need to impose some regularization on the locations of image continuities to resolve such ambiguities.

1.2. Our approach

As most images have some geometrical structures, the discontinuities of images are not randomly distributed. See Figure 1 for an illustration of the map of image edges

detected by canny edge detector. Clearly, image discontinuities (edges) are spatially correlated and there are geometrical structures in the locations of image discontinuities (see e.g. [8, 30]). Motivated by the existence of geometrical structures of image discontinuities in most images, this paper aims at developing a new regularization for image recovery which can exploit the geometrical structure of image discontinuities.

In the proposed method, the analysis operator $\mathbf{W}$ of wavelet tight frames in high-pass channels is used as the operator for detecting the image discontinuities, as the output of $\mathbf{Wf}$ measures the first-order and higher-order derivatives of images. Let Ω denote the index set of $\mathbf{Wf}$ with large amplitude, which encodes the locations of image discontinuities. Then, the index set Ω is spatially structured with certain geometric regularity owing to the existence of geometrical structures in image discontinuities. Such a geometric regularity is very helpful to facilitate the accurate estimation of Ω. Therefore, in this paper, we propose the following variational model for solving the ill-posed linear system (1):

$$\min_{\Omega,\mathbf{f}} \frac{1}{2}\|\mathbf{Af}-\mathbf{g}\|_2^2+\lambda^2\|(\mathbf{Wf})_{\Omega^c}\|_2^2 \quad \text{subject to } |\Omega|\leq t \text{ and } \Omega\in\mathcal{O}, \tag{7}$$

where $\mathbf{W}$ denotes the sparsifying operator, Ω denotes the index set of non-negligible entries of $\mathbf{Wf}$, $|\Omega|$ denotes its cardinality, and $\mathcal{O}$ denotes the feasible set for Ω that imposes additional geometric regularizations on the set Ω. The parameter λ is the regularization parameter and the parameter t determines the sparsity degree of $\mathbf{Wf}$.

To successfully apply the non-convex and non-smooth model (7) in image recovery, we need to answer the following two questions:

(1) how to effectively and efficiently solve the discrete-continuous optimization problem (7);

(2) how to design the feasible set $\mathcal{O}$ for Ω which imposes sound geometrical regularizations on image edges.

In this paper, the answer to Question 1 is to use an iterative method that alternatively updates the estimation of $\mathbf{f}$ and Ω. The answer to Question 2 in our approach is to design a feasible set for Ω which exploits one aspect of the geometric regularities on image discontinuities: the local connectivity of image edges. In our implementation, such local connectivity is characterized via the fixed point of the so-called *closing* operator (see e.g. [31]) in image morphology. Based on (7) and our answers to the two questions above, the proposed image regularization method is tested on two image recovery tasks: image deconvolution and image inpainting. The experimental results showed that the proposed method consistently outperformed several existing methods on test images.

It is noted that geometrical regularizations on image discontinuities have been studied in the context of image segmentation; see e.g [12, 41]. However, there are fundamental differences between image segmentation and image recovery. Image segmentation is more about identifying contours from image discontinuities while image recovery is more about recovering all image discontinuities from their distorted versions, e.g., sharpening image edges in image deconvolution. In other words, the discontinuities studied in image segmentation is a subset of that in image recovery, and

thus the geometrical properties of image discontinuities in image recovery are rather different from those of contours in image segmentation. In addition, only degraded images are available in image recovery while original clear images are available in image segmentation. Therefore, the geometrical regularization used in image recovery methods has to address the imperfection of detecting image discontinuities. In short, the regularization techniques on object contours studied in image segmentation is not suitable to image recovery.

1.3. Related work

In recent years, there have been an abundant literature on non-linear image recovery methods. In this section, we only give a brief review on the most related ℓ_1 norm based regularization methods. There exist three types of ℓ_1 norm based regularization methods ([23, 38]): synthesis model, analysis model and balanced model. The synthesis model assumes that an image $\mathbf{f}$ can be effectively expressed by the linear combination of only a few atoms of a synthesis system $\mathbf{D}$, i.e., $\mathbf{f} \approx \mathbf{D}\mathbf{c}$ with a sparse vector $\mathbf{c}$. Then, its variational model can be expressed as:

$$\tilde{\mathbf{f}} := \mathbf{D}\tilde{\mathbf{c}}; \quad \tilde{\mathbf{c}} := \mathrm{argmin}_{\mathbf{c}} \frac{1}{2}\|\mathbf{A}(\mathbf{D}\mathbf{c}) - \mathbf{g}\|_2^2 + \lambda\|\mathbf{c}\|_1. \tag{8}$$

The often used redundant systems $\mathbf{D}$ for synthesizing images include undecimal orthonormal wavelets [14, 15], wavelet frames [16], curvelets [8], or adaptive systems learned from images [7, 22]. The synthesis model has been used in image recovery and recognition; see e.g. [1]. The analysis model assumes that the image of interest admits a sparse projection onto an analysis system, i.e., the projection $\mathbf{\Gamma f}$ for some linear operator $\mathbf{\Gamma}$ is a sparse vector. The most often seen analysis model considers the following variational model:

$$\tilde{\mathbf{f}} := \mathrm{argmin}_{\mathbf{f}} \frac{1}{2}\|\mathbf{A}\mathbf{f} - \mathbf{g}\|_2^2 + \lambda\|\mathbf{\Gamma f}\|_1, \tag{9}$$

The most well-known analysis operators are the difference operator ∇ and its high-order extensions, which lead to the well-known total variation regularization [36]. Other often used analysis operators for sparsifying images include the analysis operator of shift-invariant wavelets [20] and that of spline wavelet frames [38]. Indeed, it is shown in [3] that, by choosing parameters properly, the wavelet frame based approaches can be seen as sophisticated discretization of minimizations involving the TV penalty and its variations.

The analysis model with either TV regularization or wavelet frame based regularization has been used in a wide rage of image recovery tasks, including deconvolution (e.g. [4, 5, 13, 33]), inpainting (e.g. [6, 17, 24, 27, 29, 37]), 3D structure reconstructions in CT and bio-imaging; see e.g. [18, 28, 39]. The balanced model [38] models an image by balancing the generativity of the synthesis model and the analysis of the analysis model, which considers the following model:

$$\tilde{\mathbf{f}} := \mathbf{W}^*\tilde{\mathbf{c}}; \quad \tilde{\mathbf{c}} := \mathrm{argmin}_{\mathbf{c}} \frac{1}{2}\|\mathbf{A}(\mathbf{W}^*\mathbf{c}) - \mathbf{g}\|_2^2 + \frac{\tau}{2}\|(I - \mathbf{W}\mathbf{W}^*)\mathbf{c}\|_2^2 + \|\mathrm{diag}(\lambda)\mathbf{c}\|_1, \tag{10}$$

where $\mathbf{W}$ denotes the analysis operator of a tight frame, λ is a given positive weighted vector and τ is a balanced parameter, $0 \leq \tau \leq \infty$. Clearly, the model (10) becomes

(8) when $\tau = 0$ and becomes (9) when $\tau = +\infty$. In addition, it is shown in [7] that in the case of denoising, the output of applying a soft/hard thresholding on wavelet frame coefficients is exactly the solution to the balanced model with ℓ_1 (or ℓ_0) norm based regularization.

In [34, 32, 40], the concept of co-sparsity is proposed to highlight the underlying difference between the synthesis model and the analysis model when being used for signal recovery. In short, what matters in the synthesis model is the support of non-zero entries of the coefficient vector $\mathbf{c}$, while what matters in the analysis model is the support of zero entries of the vector $\mathbf{\Gamma f}$. To reflect such a conceptual difference, an ℓ_0 norm based model is then discussed in [32] which can be expressed as:

$$\min \|\mathbf{\Gamma f}\|_0, \quad \text{subject to} \quad \mathbf{Af} = \mathbf{g}.$$

The minimization problem above is solved via a greedy analysis pursuit (GAP) method which iteratively updates the estimation $\mathbf{f}$ as follows:

$$\mathbf{f}_{k+1} := \operatorname{argmin} \|(\mathbf{\Gamma f})_{\Omega_k^c}\|_2^2 \quad \text{subject to } \mathbf{Af} = \mathbf{g}, \tag{11}$$

where $\mathbf{\Gamma}$ denotes the difference operator, Ω_k denotes the estimation of the support of $\mathbf{\Gamma f}$ derived from the K largest entries of $|\mathbf{\Gamma f}_k|$. Using the difference operator as $\mathbf{\Gamma}$, the GAP is applied on compressed sensing based CT reconstruction problem and showed the improvement over the traditional model (9) in the noise-free case.

Another related optimization model is proposed in [2], which aims at recovering images with piece-wise smoothness:

$$\min_{\Omega, \mathbf{f}} \frac{1}{2}\|\mathbf{Af} - \mathbf{g}\|_2^2 + \lambda \|(\mathbf{Wf})_{\Omega^c}\|_2^2 + \mu \|(\mathbf{Wf})_{\Omega}\|_1, \tag{12}$$

where $\mathbf{W}$ denotes the analysis operator of wavelet tight frame, and Ω denotes the index set of the entries of $\mathbf{Wf}$ with significant magnitude which are closely related to the locations of image edges. In other words, the optimization model (12) regularizes the smooth regions of images via the square of ℓ_2 norm based regularizer to keep it remaining smooth, and regularizes the neighborhood of jump discontinuities by the ℓ_1 norm based regularizer such that the jump discontinuities (edges) remains sharp. Furthermore, it is shown in [2] that for fixed region Ω, the discrete optimization model (12) is closely connected to the continuum variational model that generalizes the Mumford-Shah functional. In the implementation of the method for solving (12), the region Ω^c that represents the smooth regions of the piece-wise smooth function is detected via the magnitude of wavelet coefficients along several scales. The model (12) is applied on several image restoration tasks and it performs well on the image of simple edge structures, as the estimation of edge locations via wavelet coefficients for these images is easier.

The existing analysis sparse model of images is based on the sparsity prior of the discontinuities of images. All three models (8), (9) and (10) do not impose any geometric regularity constraint on the locations of the discontinuities. Such geometric regularity constraints essentially admit the spatial correlation of image gradients in the neighborhood. Such a spatial correlation of image gradients is not fully exploited in

the existing approaches. The so-called isotropic TV or $\ell_{1,2}$ norm of wavelet frame coefficients can be viewed as a regularity constraint on the correlation of image gradients along different orientations, not on the spatial correlation.

2. Minimization Model and Algorithm

Before presenting the new minimization model for image recovery, we first introduce some notations used in the remainder of the paper. The vectors and matrices are denoted by the lower and uppercase letters, and the sets are denoted by calligraphic English alphabets. For a vector $y \in \mathbb{R}^n$, y_j denotes the j-th entry. For a matrix $Y \in \mathbb{R}^{m\times n}$, $Y_i \in \mathbb{R}^n$ denotes the i-th row and $Y_{i,j}$ denotes the j-th entry of Y_i. For an index set $\Omega \subset \{1, 2, \ldots, m\}$, its cardinality, denoted by $|\Omega|$, is defined as the number of the elements of Ω. Let Y_Ω denote the sub-matrix formed by the rows of Y with indices in Ω. In this paper, we consider the analysis sparse model of images under wavelet tight frames, which has showed its effectiveness on various image restoration tasks; see e.g. [4, 6, 11, 17, 38]. Let $f \in \mathbb{R}^N$ denote the vector form of the image by concatenating all columns of $\mathbf{f}$ into a single column vector. Then the matrix representation of the analysis operator of wavelet tight frame, denoted by W, is a $MN \times N$ matrix(M is the number of the filters), whose rows of W forms a multi-level discrete tight frame for $\mathbb{R}^N$ and its transpose $W^\top$ is the synthesis operator. The perfect reconstruction property can be expressed as $W^\top W = I_N$. See Appendix A for a brief introduction of wavelet tight frames.

Consider the following ill-posed linear inverse problem:

$$g = Af + \epsilon, \tag{13}$$

where $g \in \mathbb{R}^P, f \in \mathbb{R}^N$ denote the degraded image and the image for recovery in vector form, $A \in \mathbb{R}^{P\times N}$ denotes the linear operator, and $\epsilon \in \mathbb{R}^P$ denotes measurable noise which is assumed to be i.i.d. Gaussian white noise. The analysis operator W of an un-decimal wavelet tight frame system, e.g. linear B-spline wavelet tight frame, will generate coefficients with small magnitude of image smooth regions and coefficients with large magnitude on image discontinuities. Then, based on the aforementioned discussion, one can solve (13) via solving the following optimization problem:

$$\min_f \|Af - g\|_2^2 + \|(Wf)_{\Omega^c}\|_2^2,$$

provided that the following linear system:

$$\begin{pmatrix} g \\ 0 \end{pmatrix} = \begin{pmatrix} A \\ W_{\Omega^c} \end{pmatrix} f \tag{14}$$

is invertible and well conditioned. The set Ω is the index set of those wavelet tight frame coefficients with large magnitude, and Ω^c is its complement. Clearly, the system (14) is likely to be a well-posed overcomplete system as long as there are sufficient number of entries in W_{Ω^c}. Taking image deconvolution problem for example, the matrix Af encodes the information of f in the low-pass channel, and Wf encodes the information of f in high-pass channels. The range of A and the range of W are complementary to

each other. Together with the fact that the entries of Wf on smooth image regions are close to zero, the system (14) is likely to be well-defined for most images under wavelet tight frames.

Assume that the system (14) is well-posed, we propose the following optimization model for solving (13)

$$\begin{array}{l} \min_{\Omega,f} \frac{1}{2}\|Af-g\|_2^2+\lambda\|(Wf)_{\Omega^c}\|_2^2 \\ \text{subject to } \Omega\in\mathcal{O}, \text{ and } |\Omega^c|\geq t_0 \end{array} \tag{15}$$

where λ is the regularization parameter, $\mathcal{O}$ denotes the feasible set of the index set Ω constrained by additional geometrical regularization, and Ω^c denotes the complement of Ω. The key to the success of the model (15) lies in the design of the feasible set $\mathcal{O}$ to resolve the ambiguities between Ω and f.

2.1. Design of feasible set $\mathcal{O}$

In this paper, we propose a feasible set based constraint on Ω which exploits the geometrical regularity of image discontinuities. The feasible set for Ω proposed in this paper addresses one aspect of the local geometric regularity of image edges: the strong local connectivity of wavelet frame coefficients with large magnitude. Taking image deconvolution for example, when a blurred image is deconvoluted using pesudo-inverse filter, the result usually is not satisfactory as shown in Figure 2. When checking the image pixels with large wavelet coefficients, it can be seen that image pixels with large magnitude in the result are fragmented with many small gaps, while image pixels with large magnitude in the clear image have much better connectivity. See Figure 2 for an illustration. Thus, we propose a feasible set for Ω which exploits the strong connectivity of Ω, the index set of wavelet frame coefficients with large magnitude. Such a feasible set is defined via the fixed-point of the so-called *closing* and *opening* operator in mathematical morphology (see e.g. [31]).

The closing and opening operator in binary morphology are defined on two basic operators: *dilation* and *erosion*. For an index set Ω, define its indicator binary image by

$$I_\Omega(j)=\begin{cases} 1, & \text{if } j\in\Omega; \\ 0, & \text{otherwise.} \end{cases} \tag{16}$$

Then the dilation and erosion of a binary image I_Ω are defined as

$$I_\Omega\oplus H=\mathcal{B}(I_\Omega\otimes H) \quad \text{and} \quad I_\Omega\ominus H=1-(1-I_\Omega)\oplus H^\top$$

respectively, where $\otimes$ denotes the 2D discrete convolution operator, H denotes a structure element matrix, e.g.

$$H=\begin{bmatrix} 1 & 1 & 1 \\ 1 & 1 & 1 \\ 1 & 1 & 1 \end{bmatrix},$$

and $\mathcal{B}$ denotes the binary mapping that maps any non-zero entry to 1. Then, for an index set Ω, the closing operator is defined by

$$C(\Omega,H)=\{j:((I_\Omega\oplus H)\ominus H)[j]=1\}, \tag{17}$$

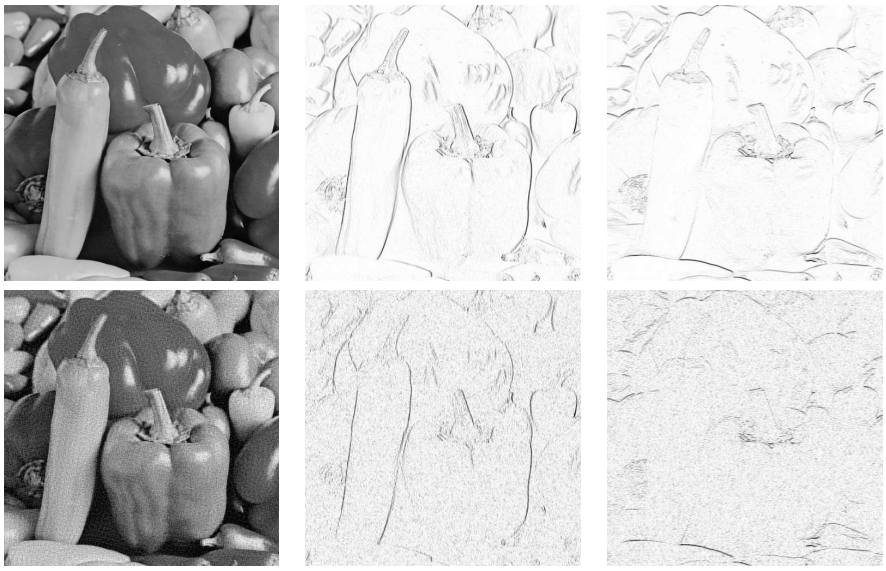

Figure 2: Comparison of the support of wavelet coefficients with large magnitude of clear image and that of the recovered one by pesudo-inverse filter. From the left to the right, the first row shows the clear image, the supports of its wavelet coefficients with large magnitude in two high-pass channels, and the second row shows the image recovered by pesudo-inverse filter, the supports of its wavelet coefficients with large magnitude in the same high-pass channels.

and the opening operator is defined by

$$O(\Omega, H) = \{j : ((I_\Omega \ominus H) \oplus H)[j] = 1\}. \tag{18}$$

The opening operator and the closing operator satisfy the duality property:

$$C(\Omega, H) = (O(\Omega^c, H^\top))^c.$$

The closing operator is used for removing small holes in a binary image for better connectivity, and thus small gaps existing in fragmented image discontinuities can be effectively filled via applying the closing operator on it.

It is known that for any index set Ω, the output $C(\Omega, H)$ after applying the closing operator on Ω is a fixed-point of $C(\cdot, H)$, i.e.,

$$C(C(\Omega, H), H) = C(\Omega, H).$$

The same also holds for the opening operator. Thus, for an index set Ω which represents the collection of wavelet coefficients with large magnitude, its connectivity property can be expressed as the fixed point of the closing operator. This motivates us to define the feasible set $\mathcal{O}$ for the index set Ω in (15) as

$$\mathcal{O} = \{\Omega : C(\Omega, H) = \Omega\}.$$

or equivalently

$$\mathcal{O} = \{\Omega^c : O(\Omega^c, H^\top) = \Omega^c\}. \tag{19}$$

Based on the definition (19), we proposed the following model for image recovery:

$$\begin{array}{l} \min_{\Omega, f} \frac{1}{2} \|Af - g\|_2^2 + \lambda \|(Wf)_{\Omega^c}\|_2^2, \\ \text{subject to } \Omega^c = O(\Omega^c), \text{ and } |\Omega^c| \geq t_0, \end{array} \tag{20}$$

where O denotes the opening operator and t_0 is some pre-defined parameter that depends on the overall percentage of image discontinuities in the image.

2.2. Numerical Algorithm

The model (20) is a challenging nonlinear non-convex mixed discrete-continuous optimization problem. Thus, we propose to solve the following relaxation form of (20):

$$\begin{array}{l} \min_{\Omega, f, \Lambda} \frac{1}{2} \|Af - g\|_2^2 + \lambda \|(Wf)_{\Lambda}\|_2^2 \\ \text{subject to } \Lambda = O(\Omega^c), \text{ and } |\Omega^c| \geq t_0 \end{array}, \tag{21}$$

where Λ is an auxiliary variable. In the next, we present a greedy pursuit based alternating iteration scheme for solving (21).

There are three variables in (21), namely f, Ω, Λ. The proposed alternating iteration scheme updates the estimation of these three variables as follows. Given $\{\Omega_k, f_k, \Lambda_k\}$,

1) update Ω_{k+1} via solving

$$\min_{\Omega} \|(Wf_k)_{\Omega^c}\|_2^2 \quad \text{subject to } |\Omega^c| \geq t_0.$$

It can be seen that the solution of the problem above is given by defining Ω_{k+1}^c as the index set of t_0 elements of $|Wf_k|$ with smallest magnitude.

2) update Λ_{k+1} by calling the opening operator on the intersection of Ω_{k+1}^c and Λ_k:

$$\Lambda_{k+1} := O({\Omega_{k+1}}^c \cap \Lambda_k).$$

3) update f_{k+1} via solving the following least squares problem:

$$\min_{f} \frac{1}{2} \|Af - g\|_2^2 + \lambda \left\|(Wf)_{\Lambda_{k+1}}\right\|_2^2. \tag{22}$$

The iteration stops when there is no more update on the estimation of Λ. See Algorithm 1 for the outline of the propose method for solving (21). It can be seen that the implementation of Algorithm 1 is simple and the computational cost in each iteration is very small.

Proposition 1. *The sequence generated by Algorithm 1 is finite and the corresponding objective function value is not increasing, i.e.,*

$$J(f_{k+1}, \Lambda_{k+1}) \leq J(f_k, \Lambda_k),$$

where J denotes the objective function of (21)*.*

Input : degraded image g; linear operator A; structure element H;
sparsity parameter t_0; regularization parameter λ;
Output: clear image f
Initial : $f_0 = g$
while $\Lambda_{k+1} \neq \Lambda_k$ **do**
(a) Ω^c_{k+1}:= the index set of t_0 smallest elements of $|Wf_k|$;
(b) $\Lambda_{k+1} := O(\Omega^c_{k+1} \cap \Lambda_k)$;
(c) $f_{k+1} = (A^TA + \lambda W^\top_{\Lambda_{k+1}} W_{\Lambda_{k+1}})^{-1} A^T g$.
end

Algorithm 1: Alternating iteration scheme for solving (21)

Proof. Let J denote the objective function of (21) such that

$$J(f, \Lambda) = \frac{1}{2} \|Af - g\|_2^2 + \lambda \|(Wf)_\Lambda\|_2^2 .$$

By the definition of Λ^{k+1}, we have

$$\Lambda_{k+1} = O(\Omega^c_{k+1} \cap \Lambda_k).$$

The anti-extensive property of the opening operator [26] gives that

$$O(\Omega^c_{k+1} \cap \Lambda_k) \subseteq \Omega^c_{k+1} \cap \Lambda_k.$$

Thus,

$$\Lambda_{k+1} = O(\Omega^c_{k+1} \cap \Lambda_k) \subseteq (\Omega^c_{k+1} \cap \Lambda_k) \subseteq \Lambda_k,$$

which leads to

$$\lambda \|(Wf)_{\Lambda_{k+1}})\|_2^2 \leq \lambda \|(Wf)_{\Lambda_k})\|_2^2,$$

then we have:

$$J(f_k, \Lambda_{k+1}) \leq J(f_k, \Lambda_k).$$

Also as f_{k+1} is the minimizer of (22), we have then

$$J(f_{k+1}, \Lambda_{k+1}) \leq J(f_k, \Lambda_{k+1}).$$

Therefore, $J(f_{k+1}, \Lambda_{k+1}) \leq J(f_k, \Lambda_k)$. In addition, as $\{\Lambda_k\}_k$ is a nested set sequence with non-increasing cardinality, Algorithm 1 will stop after a finite number of iterations due to the fact that the cardinality of all sets are bounded by the image size. □

3. Experiments

In this section, Algorithm 1 is tested on two image recovery tasks: image deconvolution and image inpainting. Let $\mathbf{f}$, $\mathbf{g}$ and $\boldsymbol{\epsilon}$ denote the original clear image, the observed degraded image and image noise respectively, and let $f \in \mathbb{R}^N, g \in \mathbb{R}^P, \epsilon \in \mathbb{R}^P$

Pepper256 Goldhill256 Boat256

Camera256 Barbara512 Lena512

Figure 3: Visualization of six test images

denote the vectorized versions of $\mathbf{f}, \mathbf{g}, \boldsymbol{\epsilon}$ respectively, then the degraded process can be modeled as follows:

$$g = Af + \epsilon, \tag{23}$$

where $A \in \mathbb{R}^{P\times N}$ is a block-wise circulant matrix under periodic boundary extension for image deconvolution problem, and is a diagonal matrix with diagonal element being 0 if the corresponding pixel being missing/damaged and 1 otherwise. The peak signal to noise ratio (PSNR) is used for the quantitative quality measurement of the results, which is defined by:

$$\mathrm{PSNR}\left(f,\bar{f}\right) = 10\log_{10}\frac{255^2}{\frac{1}{N}\sum_{i=1}^{N}\left(f_i-\bar{f}_i\right)^2},$$

where $\bar{f}$ denotes the restored image and N denotes the total number of image pixels. All numerical experiments are done in a windows 64 environment running on a PC workstation with an INTEL CPU (2.4GHZ) and 16G memory.

3.1. Experiment settings

Through all the experiments, six images are tested, as shown in Figure 3, for both image deconvolution and image inpainting. For image deconvolution, the degraded images for testing are synthesized as follows. Each test image is first convoluted by a blur kernel, followed by the addition of Gaussian white noise with different standard deviations. Four types of representative blur kernels are tested in the experiments,

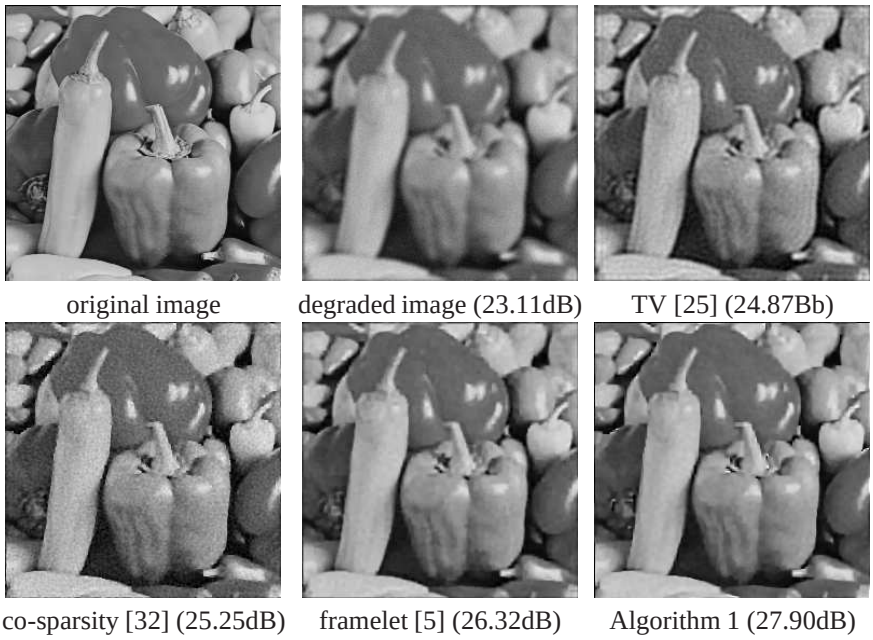

Figure 4: Visual comparison of de-blurred results for image "Peppers256". The true image is degraded by the disk kernel followed by the Gaussian noise with standard deviation $\sigma = 5$.

including (1) disk kernel of radius 3 pixels, (2) horizontal linear motion kernel of length 15 pixels, (3) Gaussian kernel of size 25×25 pixels with standard deviation $8/5$; (4) uniform averaging kernel of size 9×9 pixels. Two noise levels are tested with standard deviations $\sigma = 2, 5$.

For image inpainting, the experiments focus on recovering images whose pixel values are randomly missing, either in the absence of noise or in the presence of Gaussian white noise. Two percentages of missing pixel are tested: $r = 50\%, 70\%$, and two noise levels are tested: $\sigma = 0, 5$. In addition, two sample images are shown to demonstrate the application of image inpainting on removing texts or scratches from an input image.

3.2. Implementation details

Algorithm 1 is implemented in MATLAB R2014a. For a gray-scale image of size 256×256 pixels, the average iteration number is 8 and the average running time is around 25 seconds. The linear spline wavelet framelet [38] is used in our implementation as the system for analyzing images. There are two parameters in the proposed algorithms: λ and t_0. The optimal value of the sparsity parameter t_0 not only is related to the percentage of image smooth region, but also is related to detection accuracy of Ω. The optimal value of the regularization parameter λ is related to both the detection accuracy of Ω and the signal-to-noise-ratio of input.

For image deconvolution, the value of t_0 is determined by an auxiliary variable τ which is the estimation of the upper bound of the magnitude of the wavelet frame

original image | degraded image (20.20db) | TV [25] (24.79db)

co-sparsity [32] (24.75db) | framelet [5] (25.55db) | Algorithm 1 (25.77db)

Figure 5: Visual comparison of de-blurred results for image "Camera256". The true image is degraded by the motion kernel followed by the Gaussian noise with standard deviation $\sigma = 5$.

coefficients in smooth region, and t_0 is defined as the cardinality of the index set in which all the magnitudes of the wavelet frame coefficients are less than τ:

$$t_0 = \sharp \left\{ i | (Wf)_i \leq \tau \right\}.$$

Through all experiments in image deconvolution, the values τ and λ are set as

$$\tau = \frac{1}{3}(\sigma + 7); \quad \lambda = \frac{\sigma}{20},$$

where σ denotes the standard deviation of image noise.

For image inpainting, the detection accuracy of Ω during the iteration is different from that of image deconvolution. Through all experiments in image inpainting, the value of the sparsity parameter t_0 is set as:

$$t_0 = (1 - r/3) \times N,$$

where r denotes the percentage of missing (or damaged) pixel values and N denotes the number of image pixels. The value of the regularization parameter λ is set as:

$$\lambda = \frac{\sigma}{10},$$

where σ denotes the standard deviation of image noise. In the noise-free case, we set the value λ to a very small number: $\lambda = 0.01$.

3.3. Experiment results

To illustrate the performance gain over some related works, the results obtained from Algorithm 1 are compared to those from three most related existing image recovery methods. The first one is the total variation (TV) based regularization [36] which minimizes the ℓ_1 norm of the first-order difference of the image. The second one is the wavelet frame based regularization [5] which minimizes the ℓ_1 norm of wavelet frame coefficients of the image. These two ℓ_1 norm based regularizations are both solved via the split Bregman iteration [25]. The last one is the co-sparsity based analysis model (3) proposed in [32] which also iteratively estimates the set Ω. The main difference between the model proposed in [32] and ours lies in the additional feasible set for Ω in our model which exploits the geometrical structures embedded in Ω.

Table 1 and Table 2 summarize the results obtained from four methods when being used for image deconvolution, with respect to different configurations on the blur kernels and standard deviations of noise. It can be seen that Algorithm 1 consistently outperformed the other three methods in most cases. Compared to the two ℓ_1 norm based regularizations, including both TV based regularization and wavelet frame based regularization, Algorithm 1 has significant performance gain over the former method and has modest gain over the latter. Such a performance gain mainly comes from the better recovery of smooth image regions than the ℓ_1 norm based regularization. As images with less textures show more performance gain while images with more textures (e.g. "Barbara512") show either less performance gain or very minor to performance loss. This indicates that there are rooms for further improvement on designing better geometrical regularization on Ω when processing images of complex structures. As for the co-sparsity model [32], the performance of Algorithm 1 is noticeably better, which indicates that the ambiguities between f and Ω lead to inaccurate estimation of Ω when processing real images. In contrast, the connectivity based geometrical regularization on Ω proposed in this paper greatly alleviates such ambiguities. The visual improvement of the proposed method is also consistent with the improvement on PSNR value; see Figure 4 and Figure 5 for the visual comparison of the results on two test images.

Similar performance improvement is also observed in the experiments of image inpainting; see Table 3 for the summary of the PSNR values of the in-painted results obtained from four methods when being used for filling missing pixels values with or without noise. It can be seen that Algorithm 1 outperformed the other three methods on most test images. Again, Algorithm 1 see a minor performance loss on image "Barbara512". In addition, for the task of removing texts or scratches from input images, two images are tested; see Figure 6 and Figure 7 for the visual comparisons of the in-painted results obtained from four methods. It can be seen that the results from Algorithm 1 have the highest PSNR values and are also visually better than those from the other three methods.

4. Conclusion

The performance of sparsity-based regularizations for image recovery largely depends on the estimation accuracy of the location of image discontinuities. In order to further improve the performance of the regularization based image recovery methods,

additional regularizations on the location of image discontinuities are needed for better estimation of the locations of image discontinuities. For most images, there exist many types of geometrical structures in image discontinuities to be exploited. In this paper, we proposed a new model that considers geometrically structured approximation to images under wavelet tight frames. Moreover, by imposing connectivity constraints on wavelet frame coefficients with large magnitude, an alternating iteration scheme is developed for image recovery with simple implementation and good performance. In future, we would like to investigate more regularizations on geometrical structures of image discontinuities.

Image	Kernel	TV [25]	framelet [5]	co-sparsity [32]	Algorithm 1
Peppers256	disk	26.55	28.74	28.63	**31.12**
	motion	27.09	29.35	29.20	**30.77**
	Gaussian	26.12	26.76	25.95	**27.77**
	average	26.38	28.44	27.91	**29.24**
Goldhill256	disk	27.24	27.76	27.57	**27.98**
	motion	27.2	28.00	27.77	**28.49**
	gaussian	27.10	27.15	27.38	**27.69**
	average	26.58	26.91	26.66	**27.12**
Boat256	disk	26.41	26.58	26.95	**27.35**
	motion	26.22	27.08	26.94	**27.69**
	Gaussian	26.11	26.33	25.98	**26.70**
	average	25.37	25.71	25.26	**26.04**
Camera256	disk	26.44	27.59	27.16	**28.34**
	motion	26.15	27.78	28.10	**29.08**
	Gaussian	26.16	26.41	25.91	**27.06**
	average	25.12	25.89	25.71	**26.63**
Barbara512	disk	**25.58**	25.50	25.18	25.40
	motion	**25.05**	25.01	24.71	24.90
	Gaussian	**24.61**	24.58	24.53	24.60
	average	24.24	24.31	24.12	**24.33**
Lena512	disk	31.00	33.04	31.73	**33.04**
	motion	29.61	31.80	30.72	**32.19**
	Gaussian	32.38	33.04	32.40	**33.35**
	average	29.66	30.70	29.89	**30.90**

Table 1: Comparison of the PSNR values (dB) of the decovolution results by four methods, with respect to the noise level $\sigma = 2$.

Appendix A. Preliminaries on wavelet frames

In this section, we give a very brief introduction to the basics of frames, tight frames and wavelet tight frames in a Hilbert space $\mathcal{H}$. Interested readers are referred to ([16, 19, 38]) for more details. Let $\mathcal{H}$ denote a Hilbert space with inner product $\langle \cdot, \cdot \rangle$ and norm $\| \cdot \|$. A sequence $\{\phi_n\}_{n\in\mathbb{N}} \subset \mathcal{H}$ is a frame for $\mathcal{H}$ if there exist two positive

Image	Kernel	TV [25]	framelet [5]	co-sparsity [32]	Algorithm 1
Peppers256	disk	24.87	26.32	25.25	**27.90**
	motion	24.92	26.58	25.79	**26.72**
	Gaussian	25.08	25.97	25.08	**26.92**
	average	23.92	26.12	24.68	**26.81**
Goldhill256	disk	25.87	26.46	26.22	**26.60**
	motion	25.5	**26.28**	25.62	26.22
	Gaussian	26.06	26.41	26.30	**26.80**
	average	24.93	25.61	25.20	**25.62**
Boat256	disk	24.638	25.41	24.85	**25.50**
	motion	24.17	25.02	24.2	**25.08**
	Gaussian	24.96	25.51	24.94	**25.62**
	average	23.64	**24.43**	23.78	24.40
Camera256	disk	24.43	25.68	24.53	**25.87**
	motion	23.65	25.35	24.74	**25.63**
	Gaussian	24.79	25.55	24.75	**25.77**
	average	23.17	24.51	23.68	**24.76**
Barbara512	disk	24.21	24.15	24.29	**24.34**
	motion	23.57	23.88	23.57	**23.93**
	Gaussian	24.09	24.26	24.11	**24.24**
	average	23.45	23.69	23.49	**23.71**
Lena512	disk	29.94	30.17	31.16	**31.19**
	motion	27.69	29.33	28.32	**29.41**
	Gaussian	30.45	31.53	30.70	**31.64**
	average	28.07	29.17	28.44	**29.18**

Table 2: Comparison of the PSNR values (dB) of the deconvolution results by four methods, with respect to the noise level $\sigma = 5$.

constants a and b such that

$$a\|f\|_2^2 = \sum_{n\in\mathbb{N}} |\langle \phi_n, f\rangle|^2 \leq b\|f\|_2^2, \quad \forall\, f \in \mathcal{H}.$$

A frame $\{\phi_n\}_{n\in\mathbb{N}}$ is called a tight frame for $\mathcal{H}$ when $a = b = 1$. There are two operators associated with a given frame $\{\phi_n\}_{n\in\mathbb{N}}$: the analysis operator $\mathbf{W}$ defined by

$$\mathbf{W} : f \in \mathcal{H} \longrightarrow \{\langle f, \phi_n\rangle\} \in \ell^2(\mathbb{N})$$

and its adjoint operator $\mathbf{W}^*$, also called the synthesis operator, defined by

$$\mathbf{W}^* : \{a_n\} \in \ell^2(\mathbb{N}) \longrightarrow \sum_n a_n\phi_n \in \mathcal{H}.$$

The concatenation of these two operators forms a so-called frame operator $\mathbf{F} = \mathbf{W}^*\mathbf{W}$ given by

$$\mathbf{F} : f \in \mathcal{H} \longrightarrow \sum_{n\in\mathbb{N}} \langle f, \phi_n\rangle\phi_n.$$

Image	(r, σ)	TV [25]	framelet [5]	co-sparsity [32]	Algorithm 1
Pepper256	(0.5,0)	28.32	30.49	27.64	**31.10**
	(0.5,5)	27.65	29.51	27.09	**29.94**
	(0.7,0)	25.33	26.07	25.05	**26.45**
	(0.7,5)	25.13	25.77	24.81	**26.23**
Goldhill256	(0.5,0)	29.20	29.81	28.79	**29.90**
	(0.5,5)	28.40	28.96	28.08	**29.14**
	(0.7,0)	26.49	27.20	26.31	**27.28**
	(0.7,5)	26.17	26.82	26.00	**26.93**
Boat256	(0.5,0)	27.63	28.46	27.73	**28.58**
	(0.5,5)	27.07	27.84	27.16	**27.97**
	(0.7,0)	24.65	25.58	25.15	**25.73**
	(0.7,5)	24.45	25.33	24.90	**25.46**
Camera256	(0.5,0)	27.65	28.54	27.54	**28.82**
	(0.5,5)	27.11	27.94	26.99	**28.31**
	(0.7,0)	24.63	**25.38**	24.71	25.32
	(0.7,5)	24.41	**25.16**	24.49	25.15
Barbara512	(0.5,0)	26.39	**27.46**	26.86	27.40
	(0.5,5)	25.97	**26.97**	26.39	26.96
	(0.7,0)	24.47	**25.02**	24.71	24.83
	(0.7,5)	24.27	**24.81**	24.5	24.65
Lena512	(0.5,0)	34.36	35.24	34.13	**35.34**
	(0.5,5)	32.16	33.04	32.06	**33.35**
	(0.7,0)	30.76	**31.92**	30.94	31.75
	(0.7,5)	29.91	**30.99**	30.10	30.95

Table 3: Comparison of the PSNR values (dB) of the inpainting results by four methods, with respect to different percentages of missing pixel values and different noise levels.

It can be seen that a sequence $\{\phi_n\}_{n\in\mathbb{N}} \subset \mathcal{H}$ forms a tight frame if and only if $\mathbf{F} = \mathbf{I}$, where $\mathbf{I} : \mathcal{H} \longrightarrow \mathcal{H}$ is the identity operator. Generally speaking, frames and tight frames are the generalizations of Riesz bases and orthonormal bases to redundant systems. Indeed, a tight frame $\{\phi_n\}_{n\in\mathbb{N}}$ also satisfies the same *perfect reconstruction property* as an orthonormal basis:

$$f = \sum_{n\in\mathbb{N}} \langle f, \phi_n\rangle \phi_n, \quad \forall\, f \in \mathcal{H}. \tag{A.1}$$

In addition, it forms an orthonormal basis for $\mathcal{H}$ if $\|\phi_n\| = 1$ for all ϕ_n.

Wavelet tight frames are widely used in signal/image processing owing to the effectiveness on sparse image modeling and the efficiency on related computations. A wavelet tight frame for $L_2(\mathbb{R})$ is a system formed by the shifts and dilations of a finite set of a few generators $\Psi = \{\psi_1, \ldots, \psi_m\} \subset L_2(\mathbb{R})$:

$$X(\Psi) = \{2^{j/2}\psi_\ell(2^j \cdot -k), \quad 1 \le \ell \le m, j \in \mathbb{Z}, k \in \mathbb{Z}\}.$$

One approach to construct wavelet tight frame is via the so-called *multi-resolution analysis*, which starts with a scaling function ϕ with $\widehat{\phi}(0) = 1$ that satisfies the following refinable equation $\widehat{\phi}(2\cdot) = \widehat{a_0}\widehat{\phi}$, where $\widehat{\phi}$ is the Fourier transform of ϕ, and $\widehat{a_0}$ is a

Figure 6: Visual comparison of in-painted results for image "Lena512" when removing the scratches and texts by four methods.

2π-periodic trigonometric polynomial:

$$\widehat{\phi}\,(\omega) = \int_{\mathbb{R}} \phi(t) e^{-i\omega t} \mathrm{dt}, \mathrm{t} \in \mathbb{R}$$

$$\widehat{a_0}(\omega) := \sum_{k\in\mathbb{Z}} a_0(k) e^{-ik\omega}$$

with $\widehat{a_0}(0) = 1$. Then each generator ψ_ℓ is defined by $\widehat{\psi_\ell} = \widehat{a_\ell}\widehat{\phi}, \quad 1 \le \ell \le m$. The so-called *Unitary Extension Principle* [35] which says that $X(\Psi)$ forms a tight frame if $\phi \in L^2(\mathbb{R})$ and

$$\sum_{\ell=0}^{m} \widehat{a}_\ell(\omega)\overline{\widehat{a_\ell}(\omega)} = 1, \quad \text{and} \quad \sum_{\ell=0}^{m} \widehat{a}_\ell(\omega)\overline{\widehat{a_\ell}(\omega+\pi)} = 0. \tag{A.2}$$

One such example often used image recovery is the linear B-spline frame [16] for $L^2(\mathbb{R})$, which has one scaling function and two wavelets and the associated masks $\{a_0, a_1, a_2\}$ are

$$a_0 = \frac{1}{4}[1,2,1]; \quad a_1 = \frac{\sqrt{2}}{4}[1,0,-1]; \quad a_2 = \frac{1}{4}[-1,2,-1]. \tag{A.3}$$

The framelet system for $L_2(\mathbb{R}^2)$ can be obtained by taking the tensor product of univariate framelets. In the discrete setting, for a given frame $\{\phi_n\}_{n=1}^M \subset \mathbb{R}^N$, the matrix

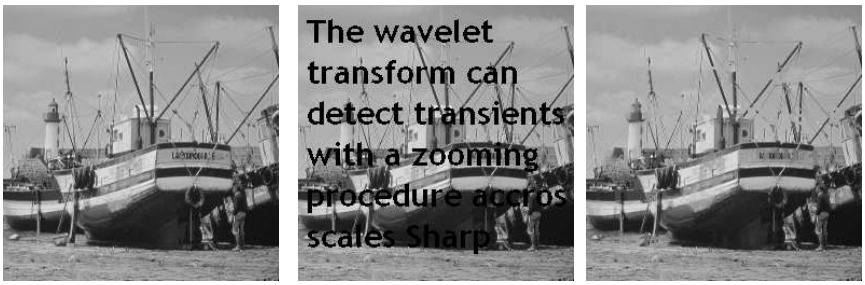

original image | degraded image | TV [25] (29.88 dB)

co-sparsity [32] (30.62 dB) | framelet [5] (30.95 dB) | Algorithm 1 (31.06 dB)

Figure 7: Visual comparison of the inpainting results for image "Boat256" when removing texts by four methods.

representation of the associated analysis operator is $W = (\phi_1, \phi_2, \ldots, \phi_M)^\top$ and the synthesis operator is its transpose $W^\top$. Clearly, $\{\phi_n\}_{n=1}^M$ forms a frame for $\mathbb{R}^N$ if and only if $W^\top W$ is non-singular and it forms a tight frame if and only if $W^\top W = I_N$, where I_N is the N-by-N identical matrix.

The wavelet tight frame for $\mathbb{R}^N$ can be constructed from the masks associated with the framelets for the space of continuum. For simplicity, only L-level un-decimal wavelet tight frame systems for $\mathbb{R}^N$ are introduced here. Let a_0 denote the mask associated with the scaling function and $\{a_1, a_2, \ldots, a_m\}$ denote the masks associated with other framelets. Then, the low-pass filter $a_0^{(\ell)}$ at the level ℓ is define as

$$a_0^{(\ell)} = a_0^{\downarrow_1} * a_0^{\downarrow_2} * \cdots * a_0^{\downarrow_{2^{\ell-1}}},$$

where $*$ denotes the discrete convolution operator and

$$a_0^{\downarrow_{2^\ell}} = [\ldots, a_0(-2), \overbrace{0, \ldots, 0}^{2^\ell-1}, a_0(-1), \overbrace{0, \ldots, 0}^{2^\ell-1}, a_0(0), \overbrace{0, \ldots, 0}^{2^\ell-1}, a_0(1), \overbrace{0, \ldots, 0}^{2^\ell-1}, a(2), \ldots].$$

Then, for the level $\ell = 1, \ldots, L-1$, the corresponding filter set is $\{a_k^{(\ell)}\}_{k=1}^m$ where

$$a_k^{(\ell)} = a_0^{(\ell-1)} * a_k.$$

For the L-th level, the filters are $\{a_k^{(L)}\}_{k=1}^m \cup a_0^{(L)}$.

Let $f \in \mathbb{R}^N$ denote the vector form of the image by concatenating all columns of $\mathbf{f}$ into a single column vector. For a given filter a of finite length, Let the N-by-N matrix, denoted by S_a, be the Toeplitz-plus-hankel matrix that represents the convolution operator by the mask a under Neumann boundary condition (see [10]). Then, the analysis operator of a L-level discrete wavelet tight frame can be expressed as

$$W = [W_1^\top, W_2^\top, ..., W_L^\top]^\top, \tag{A.4}$$

where W_ℓ denotes the ℓ-th level analysis operator defined by

$$W_\ell = [S^\top_{a_1^{(\ell)}}, S^\top_{a_2^{(\ell)}}, \ldots, S^\top_{a_m^{(\ell)}}]^\top, \quad \ell = 1, 2, \ldots, L-1, \tag{A.5}$$

and $W_L = [S^\top_{a_1^{(L)}}, S^\top_{a_2^{(L)}}, \ldots, S^\top_{a_m^{(L)}}, S^\top_{a_0^{(L)}}]^\top$. The rows of W forms a multi-level tight frame for $\mathbb{R}^N$ and its transpose $W^\top$ is the synthesis operator. The perfect reconstruction property in matrix representation can be expressed as $W^\top W = I_N$.

Acknowledgment

The authors would like to thank the associate editor and the reviewers for their helpful comments and suggestions. This work was partially supported by Singapore MOE AcRF Research Grant MOE2011-T2-1-116 and R-146-000-165-112.

References

[1] Aharon, M., Elad, M., Bruckstein, A., 2006. K-SVD: An algorithm for designing overcomplete dictionaries for sparse representation. IEEE Trans. Image Process. 54 (11), 4311–4322.

[2] Cai, J., Dong, B., Shen, Z., 2014. Image restorations: a wavelet frame based model for piecewise smooth functions and beyond. CAM report 14-28, UCLA.

[3] Cai, J., Dong, B., Shen, Z., Osher, S., 2012. Image restoration: total variation; wavelet frames; and beyond. J. Am. Math. Soc. 25 (4), 1033–1089.

[4] Cai, J., Ji, H., Liu, C., Shen, Z., 2012. Framelet based blind image deblurring from a single image. IEEE Trans. Image Process. 21 (2), 562–572.

[5] Cai, J., Osher, S., Shen, Z., 2009. Split bregman methods and frame based image restoration. SIAM Multiscale Model. Simul. 8 (2), 337–369.

[6] Cai, J.-F., Chan, R., Shen, Z., 2008. A framelet-based image inpainting algorithm. Appl. Comput. Harmon. Anal. 24, 131–149.

[7] Cai, J. F., Ji, H., Shen, Z., Ye, G. B., 2014. Data-driven tight frame construction and image denoising. Appl. Comput. Harmon. Anal. 37 (1), 89–105.

[8] Candes, E., Donoho, D. L., 2002. New tight frames of curvelets and optimal representations of objects with piecewise-C^2 singularities. Comm. Pure Appl. Math 57, 219–266.

[9] Candès, E. J., Fernandez-Granda, C., 2014. Towards a mathematical theory of super-resolution. Comm. Pure Appl. Math. 67 (6), 906–956.

[10] Chan., R., Riemenschneider, S., Shen, L., Shen, Z., 2004. Tight frame: an efficient way for high-resolution image reconstruction. Appl. Comput. Harmon. Anal. 17, 91–115.

[11] Chan, R. H., Chan, T. F., Shen, L., Shen, Z., 2003. Wavelet algorithms for high-resolution image reconstruction. SIAM J. Sci. Comput. 24, 1408–1432.

[12] Chan, T., Vese, L., 2001. Active contours without edges. IEEE Trans. Image Process. 10.2 (2001): 266-277. 10 (2), 266–277.

[13] Chan, T., Wong, C., 1998. Total variation blind deconvolution. IEEE Trans. Image Process. 7 (3), 370–375.

[14] Coifman, R., Donoho, D., 1994. Translation-invariant de-noising. Wavelet and Statistics. Vol. 103 of Springer Lecture Notes in Statistics. Springer-Verlag., pp. 125–150.

[15] Daubechies, I., 1992. Ten lectures on wavelets, 1st Edition. CBMS-NSF Lecture Notes, SIAM.

[16] Daubechies, I., Han, B., Ron, A., Shen, Z., 2003. Framelets: MRA-based constructions of wavelet frames. Appl. Comput. Harmon. Anal. 14, 1–46.

[17] Dong, B., Ji, H., Li, J., Shen, Z., 2012. Wavelet frame based blind image inpainting. Appl. Comput. Harmon. Anal. 32 (2), 268–279.

[18] Dong, B., Li, J., Shen, Z., 2013. X-ray ct image reconstruction via wavelet frame based regularization and radon domain inpainting. SIAM J. Sci. Comput. 54(2-3) (2013), 333-349. 54 (2), 333–349.

[19] Dong, B., Shen, Z., 2010. MRA based wavelet frames and applications. IAS Lecture Notes Series, Summer Program on "The Mathematics of Image Processing", Park City Mathematics Institute.

[20] Donoho, D., 1995. De-noising by soft thresholding. IEEE Trans. Inf. Theory 41 (3), 613–627.

[21] Donoho, D., 2006. Compressed sensing. IEEE Trans. Inf. Theory 52 (4): 1289. 52 (4).

[22] Elad, M., Ahron, M., 2006. Image denoising via sparse and redundant representations over learned distionaries. IEEE Trans. Image Process. 54 (12), 3736–3745.

[23] Elad, M., Milanfar, P., Rubinstein, R., 2007. Analysis versus synthesis in signal priors. Inverse Probl. 23 (3), 947–968.

[24] Elad, M., Starck, J.-L., Querre, P., Donoho, D. L., 2005. Simultaneous cartoon and texture image inpainting using morphological component analysis (mca). Appl. Comput. Harmon. Anal. 19 (3), 340–358.

[25] Goldstein, T., Osher, S., 2009. The split bregman method for l1-regularized problems. SIAM J. Img. Sci. 2 (2), 323–343.

[26] Haralick, R. M., Sternberg, S. R., Zhuang, X., 1987. Image analysis using mathematical morphology. IEEE Trans. Pattern Anal. Mach. Intell. (4), 532–550.

[27] King, E. J., Kutyniok, G., Zhuang, X., 2014. Analysis of inpainting via clustered sparsity and microlocal analysis. J. Math. Imaging Vision 48 (2), 205–234.

[28] Li, M., Fan, Z., Ji, H., Shen, Z., 2014. Wavelet frame based algorithm for 3d reconstruction in electron microscopy. SIAM J. Sci. Comput. 36 (1), 45–69.

[29] Li, Y.-R., Shen, L., Suter, B. W., 2013. Adaptive inpainting algorithm based on dct induced wavelet regularization. IEEE Trans. Image Process. 22 (2), 752–763.

[30] Mallat, S., Lepennec, E., 2005. Sparse geometric image representation with bandelets. IEEE Trans. Image Process. 14, 423–438.

[31] Najman.L, Talbot, H. (Eds.), 2010. Mathematical morphology: from theory to applications. ISTE-Wiley.

[32] Nam, S., Davies, M., Elad, M., 2013. The cosparse analysis model and algorithms. Appl. Comput. Harmon. Anal. 34 (1), 30–56.

[33] Osher, S., Burger, M., Goldfarb, D., Xu, J., Yin, W., 2005. An iterative regularization method for total variation-based image restoration. SIAM Multiscale Model. Simul. 4 (2), 460–489.

[34] Peleg, T., Elad, M., 2013. Performance guarantees of the thresholding algorithm for the co-sparse analysis model. IEEE Trans. Inf. Theory 59 (3), 1832–1845.

[35] Ron, A., Shen, Z., 1997. Affine system in $L_2(R^d)$: the analysis of the analysis operator. J. Func. Anal. 148.

[36] Rudin, L., Osher, S., Fatemi, E., 1992. Nonllienar total variation based noise removal algorithms. Phys. D. 60, 259–268.

[37] Shen, J., Chan, T. F., 2002. Mathematical models for local nontexture inpaintings. SIAM J. Appl. Math. 3 (62), 1018–1043.

[38] Shen, Z., 2010. Wavelet frames and image restorations. Proceedings of the International Congress of Mathematicians, Hyderabad, India.

[39] Sidky, E. Y., Pan, X., 2008. Image reconstruction in circular cone-beam computed tomography by constrained total-variation minimization. Phys. Med. Biol. 53 (17), 4777.

[40] Turek, J. S., Yavneh, I., Elad, M., 2014. On MAP and MMSE estimators for the co-sparse analysis model. DSP 28, 57–74.

[41] Vese, L., Chan, T., 2002. A multiphase level set framework for image segmentation using the mumford and shah model. Int. J. Comput. Vis. 50 (3), 271–293.